Supporting Information

Backbone Flexibility/Amphiphilicity Modulation of AIE Active Polyelectrolytes for Mitochondria-and-Nucleus-Targeted Synergistic Photodynamic Therapy of Cancer Cells

Zhiguo He[a,b,‡], Xuejiao Han[a,c‡], Zifeng Yan[b], Bing Guo[,a], Qiang Cai[d], Youwei Yao[b]*

[a] School of Science, Shenzhen Key Laboratory of Flexible Printed Electronics Technology, Harbin Institute of Technology, Shenzhen 518055, China. Email: guobing2020@hit.edu.cn

[b] Institute of Materials Research, Shenzhen International Graduate School, Tsinghua University, Shenzhen, 518055, China

[c] Department of Medical Oncology, Harbin Medical University Cancer Hospital, Harbin 150081, China

[d] School of Materials Science and Engineering, Tsinghua University, Beijing, China, 100084, China

1 Materials and Methods

1.1 Materials

4-Bromo-N-(4-bromophenyl)-N-phenylaniline, pyridin-4-ylboronic acid, 4-vinylpyridine, Potassium carbonate (K_2CO_3), Palladium acetate ($Pd(OAc)_2$), Triphenylphosphine ($P(C_6H_5)_3$), Triethylamine (TEA), 1,4-dibromobutane, 1,6-dibromohexane, dimethylformamide (DMF), Tetrahydrofuran (THF), dimethyl sulfoxide (DMSO), 9,10-Anthracenediyl-bis(methylene)-dimalonic acid (ABDA) were obtained from Macklin. Tetrakis(triphenylphosphine)palladium (0) ($Pd[P(C_6H_5)_3]_4$), Rose Bengal (RB), and Phosphate buffer saline (PBS) were purchased from Aladdin. They were used without further purification unless otherwise stated. The biochemical reagents including culture medium and other components were supplied by Boyetime Biotechnology. Cell assays like CCK8 kit and DAPI and mito-tracker Red were purchased from Boyetime Biotechnology.

1.2 Measurements

NMR spectra were determined on a Bruker 400NMR spectrometer with tetramethylsilane (TMS, δ = 0 ppm) as an internal standard. High-resolution mass spectra (HRMS) were performed on Waters Xevo TQD with an ESI source. The UV-vis absorption spectra were recorded by Uv-vis spectrophotometer (UV-2600, SHIMADZU). PL emission spectra were recorded a spectrofluorometer (Fluoro Max-4). DLS test was conducted on Malvern Nanoziser (Zetasizer Nano ZSP) at ambient temperature. The morphology of the molecule was observed using a JEOL JSM-6700F type transmission Electron Microscope (TEM). The zeta potential of the sample was measured by the Malvern Zetasizer Nano ZS90 instrument at room temperature. Fluorescence lifetime was obtained with a Transient fluorescence spectrometer (FLS 1000, Edinburgh Instruments). Cell imaging photos were taken with Confocal laser scanning microscopy (CLSM, Nikon).

1.3 Calculation of photophysical properties

PLQYs are obtained with by a relative method with the alcohol solution of Rhodamine B as reference. The data were obtained by **equation S1**:

$$\Phi_S = \frac{n_S^2}{n_R^2} * \frac{A_R * F_S}{A_S * F_R} * \Phi_R \qquad \text{S1}$$

Where Φ_S, Φ_R is the PLQY of sample and reference sample, *i.e.* Rhodamine B alcohol solution; n_S ,n_R is the reflective index of the solvents of sample and reference sample, respectively. A_R and A_S represent the absorbance of the reference sample and sample at the excitation wavelength (450 nm).

The fluorescence lifetime was calculated by following procedures. First, the transient PL spectra were fitted by by ExpDec2 (**Equation S2**) or ExpDec3 (**Equation S3**) functions, which depends on the p value. And the derived parameters were used to obtain the fluorescence were then applied to **Equation S4** or **S5** accordingly to obtain the fluorescence lifetime:

$$ExpDec(t) = A_1 e^{\frac{-t}{\tau_1}} + A_2 e^{\frac{-t}{\tau_2}} \qquad \text{S2}$$

$$ExpDec(t) = A_1 e^{\frac{-t}{\tau_1}} + A_2 e^{\frac{-t}{\tau_2}} + A_3 e^{\frac{-t}{\tau_3}} \qquad \text{S3}$$

$$\tau = \frac{A_1\tau_1^2 + A_2\tau_2^2}{A_1\tau_1 + A_2\tau_2} \qquad \text{S4}$$

$$\tau = \frac{A_1\tau_1^2 + A_2\tau_2^2 + A_3\tau_3^2}{A_1\tau_1 + A_2\tau_2 + A_3\tau_3} \qquad \text{S5}$$

And the radiative decay rate and non-radiative decay are derived by **Equation S6** and **S7**.

$$\eta = \frac{\Gamma}{\Gamma + \kappa_{nr}} \qquad \text{S6}$$

$$\tau = \frac{1}{\Gamma + \kappa_{nr}} \qquad \text{S7}$$

1.4 Simulation methods

The ground state geometry is optimized using DFT, and the excited states are calculated with linear response time-dependent DFT (TDDFT) at the optimized ground state geometry. All calculations are performed with the Gaussian 16 package (Rev. C.01) using the hybrid B3LYP functional

For geometry optimization calculations, the def2-SVP basis set was used, and the optimal geometry for each compound was determined. The excited states calculations were performed with a larger basis set def2-TZVP basis set.

Grimme's D3BJ dispersion correction was used to improve calculation accuracy.

Orbital energy level analysis was performed by Multiwfn software.

1.5 ROS production monitoring

To study the ROS generation efficiency of, ABDA was used to detect the ROS generation upon light irradiation. The ABDA solution (concentration = 100 μM) was mixed with different compounds (concentration = 10 μM) in water and exposed to LED white light illumination (400-700 nm) at a power density of 70 mW/cm^2 for different time. The decomposition of ABDA was monitored by ultraviolet spectrometry at 400 nm.

1.6 ROS quantum yield measurements.

The ROS quantum yield of different compounds in water (Φ) was measured using ABDA as an indicator and Bengal rose (RB) as a standard reference and calculated by **Equation S8**.

$$\Phi_S = \frac{\Phi_{RB}(K_S \bullet A_{RB})}{K_{RB} \bullet A_S} \qquad \text{S8}$$

Where K_S and K_{RB} are the decomposition rate constants of the photosensitizing process determined by the plot ln (A_0/A) versus irradiation time. A_0 is the initial absorbance of ABDA while A is the ABDA absorbance after different irradiation times. A_S and A_{RB} represent the light absorbed by the samples and RB, which are determined by the integration of the absorption bands in the wavelength range of 400-700 nm. Φ_{RB}

is the ROS quantum yield of RB, which is 0.75 in water. The calculation procedures are as follows:

Table S1 ROS quantum yields calculation procedures.

Sample	A_s	K_s	Φ_S
S4	19.21622918	0.01518	0.99
S6	14.888205	0.01484	1.26
D4	31.97282215	0.03743	1.47
D6	29.7515585	0.04543	1.92
SD4	7.356538458	0.01208	2.06
RB	24.1957132	0.01444	0.75

2 In vitro experiments

2.1 Cell culture

U87, A549, HepG2, HepG1-6, HACAT cells were supplied by Perkin Elmer Inc. and maintained in our lab. U87, A549, HepG1-6 cells were cultured on 10 cm dishes in Eagle's minimal essential medium (DMEM, with 10% fetal bovine serum (FBS), 1% penicillin/streptomycin), while HepG2 cells were cultured in Minimum Essential Medium (MEM), with with 10% fetal bovine serum (FBS), 1% penicillin/streptomycin), 1% sodium pyruvate, 1% GlutaMax, 1% MEM NEAA. The cells were maintained in an atmosphere of 5% CO2 and 95% humidified air at 37 °C.

2.2 Cell imaging

Above cells were respectively seeded and cultured in confocal dishes at a density of 300, 000 cells per dish for 24 h. Then culture mediums were then replaced by fresh

medium containing 2μM the AIE polyelectrolytes and incubated for certain hours. Subsequently, mito-tracker Red was added into the medium with a similar procedure and cultured for 30 min, the then and cells were fixed by paraformaldehyde, after which the fixed cells were stained by DAPI and washed by PBS twice. The fluorescent signal of the AIE polyelectrolytes inside cells was captured by confocal laser scanning microscopy (CLSM) (Leica TSC SP8, Germany) with excitation at 488 nm and signal collection from 500-540 nm. The fluorescent signal of DAPI inside cells was captured with excitation at 405 nm and signal collection from 430-470 nm. The fluorescent signal of Mitochondrial Red inside cells was captured with excitation at 561 nm and collection from 560-600 nm.

2.3 Intracellular ROS detection

The intracellular ROS generation was monitored by the aid of a commercial ROS detection fluorescent probe, 2,7-Dichlorodihydrofluorescein diacetate (DCFH-DA).
It undergoes hydrolysis and oxidation when enters cells, thus emitting bright fluorescent signals, which can be harvested as a measurement for intracellular ROS level. The operation was guided by the instruction book offered by the supplier (Beyotime). Namely, the after cells were cultured for 24 h in confocal dishes then the AIE polyelectrolytes were charged into fresh medium to replace the used culture medium. After another 12-hour culture, DCFH-DA (10 μM) was added in the confocal dishes by a similar procedure. Then the cell was incubated for 20 min (5% CO_2, 37℃), which was followed by LED illumination for 5 min (70 mW/cm^2), PBS rinse and fixation by paraformaldehyde. the fluorescence signal was captured by CLSM and analyzed by Image J software.

2.4 Cytotoxicity measurement

The quantitative cytotoxicity of TPA polyelectrolytes in the presence or absence of white LED illumination was obtained by a strandard CCK assay. U87 glioma cancer cells were seeded in 96-well plates with a concentration of 10000 cells per well. After 24-hour incubation, the AIE polyelectrolytes were charged by replacing the culture

medium with fresh mediums containing the AIE polyelectrolyte at certain concentration (0, 0.5, 1, 2, 5, 10 μM). Then the plates were placed back in the incubation box for another 12 h, which was followed by illumination of LED white light (70 mW/cm^2, 5 min) and a further culture for another 12 h. Then CCK was added and the cells were maintained in incubation for another 2 h, followed by the cytotoxicity test by the aid of microplate reader.

3 Synthesis

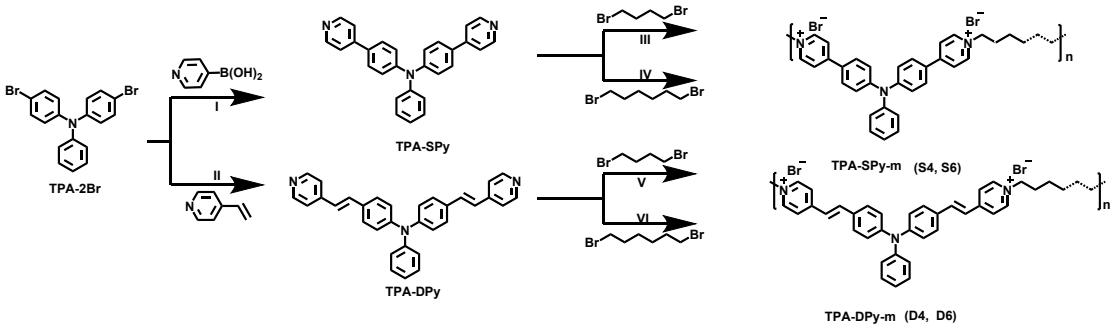

Scheme S1 Synthetic routes of the AIE polyelectrolytes.

3.1 Synthesis of TPA-SPy.

TPA-containing precursor **TPA-SPy** was synthesized following a modified procedure.[1] 4-Bromo-N-(4-bromophenyl)-N-phenylaniline (TPA-2Br) (418 g mol^{-1}, 0.5 mmol, 209 mg), pyridin-4-ylboronic acid (123 g mol^{-1}, 1.5 mmol, 184.3 mg), $Pd[P(C_6H_5)_3]_4$ (1155 g mol^{-1}, 0.05 mmol, 57.8 mg), and K_2CO_3 (138 g mol^{-1}, 2 mmol, 276 mg) were dissolved in mixture of THF and H_2O (30 mL, V_{THF}:V_{water} = 2:1). Then, the mixture was refluxed at 120 °C for 24 h under argon protection, and then stirred for another 30 min at room temperature. The solvent was removed using rotary evaporator and filtered with CH_2Cl_2. The filtrate was removed using rotary evaporator and resultant crude compound was purified by silica gel column chromatography with hexane/THF by volume of 2:1 to obtain the yellow pure **TPA-SPy** with 62.1 % yield.

3.2 Synthesis of TPA-DPy.

TPA-2Br (209.07 mg, 0.5 mmol), 4-vinyl-pydine (105.14 mg, 1.5 mmol), Pd(OAc)2

(11.22 mg, 0.05 mmol), P(otyl)3 (45.66 mg, 0.15 mmol), triethylamine 4mL, DMF 2mL were added into a 50 mL flask, separately. And then the air in the flask was removed by three times of argon-air exchange, and at last the flask was protected with an argon balloon, then heated to 90 ℃ and kept for 48 h. When the system cooled to ambient temperature, the solvent was removed by rotating evaporation. And the product was obtained as bright yellow powders with the purification of a silica gel column chronmatography (eluent (v/v) hexane/THF =3:2).

3.3 Synthesis of TPA-SPy-4.

A Schlenk tube was charged with **TPA-SPy** (100 mg, 0.2214 mmol) and 10 mL DMF. and then 1,4-dibromobutane (47.82 mg, 0.2214 mmol) were added into the Schlenk tube. The mixture was refluxed at 80 °C for 36 h under argon protection and then stirred for another 30 min at room temperature. The solvent was removed using rotary evaporator. All products were washed by 10 mL THF and 10 mL hexane for 5 times to obtain the corresponding cationic polymers TPA-S4 as a yellow solid with 49.2% yield.

3.4 Synthesis of TPA-SPy-6, TPA-DPy-4, TPA-DPy-6

TPA-SPy-6 (57.2%), **TPA-DPy-4** (54.3%) and **TPA-DPy-6** (49.2%) were obtained by a similar method.

Supplementary Figures

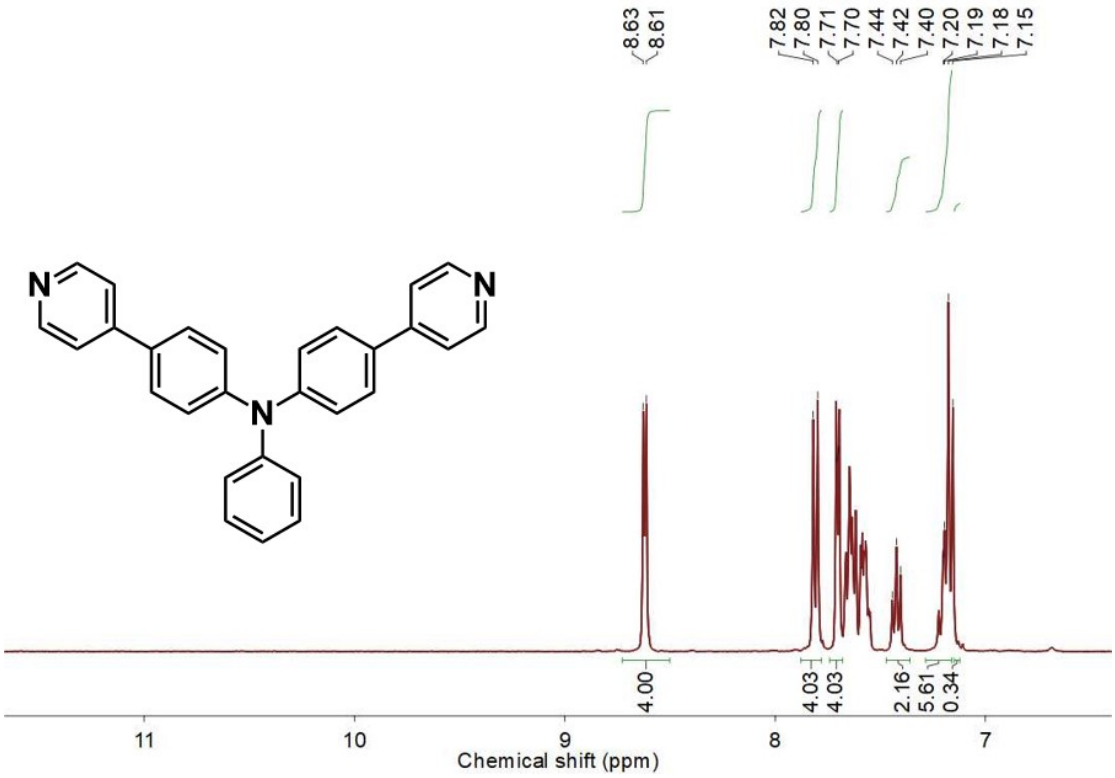

Figure S1. ^{1}H NMR spectrum of **TPA-SPy** in $CDCl_3$.

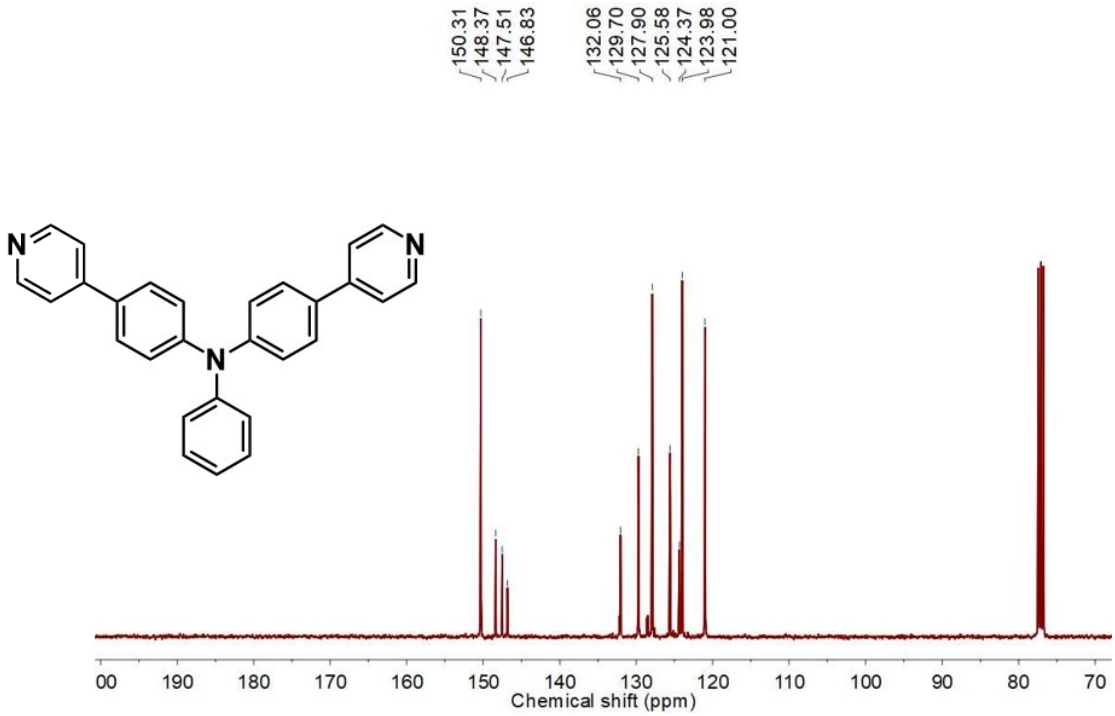

Figure S2. ^{13}C NMR spectrum of **TPA-SPy** in $CDCl_3$

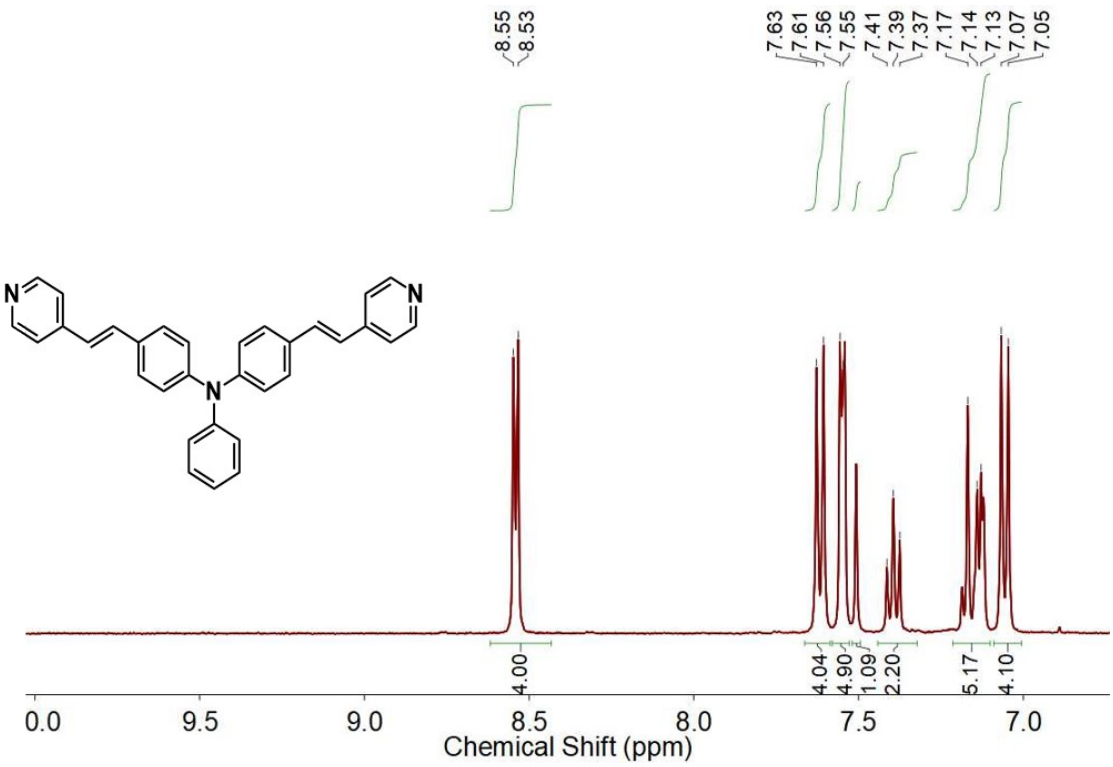

Figure S3. ^{1}H NMR spectrum of **TPA-DPy** in $CDCl_3$

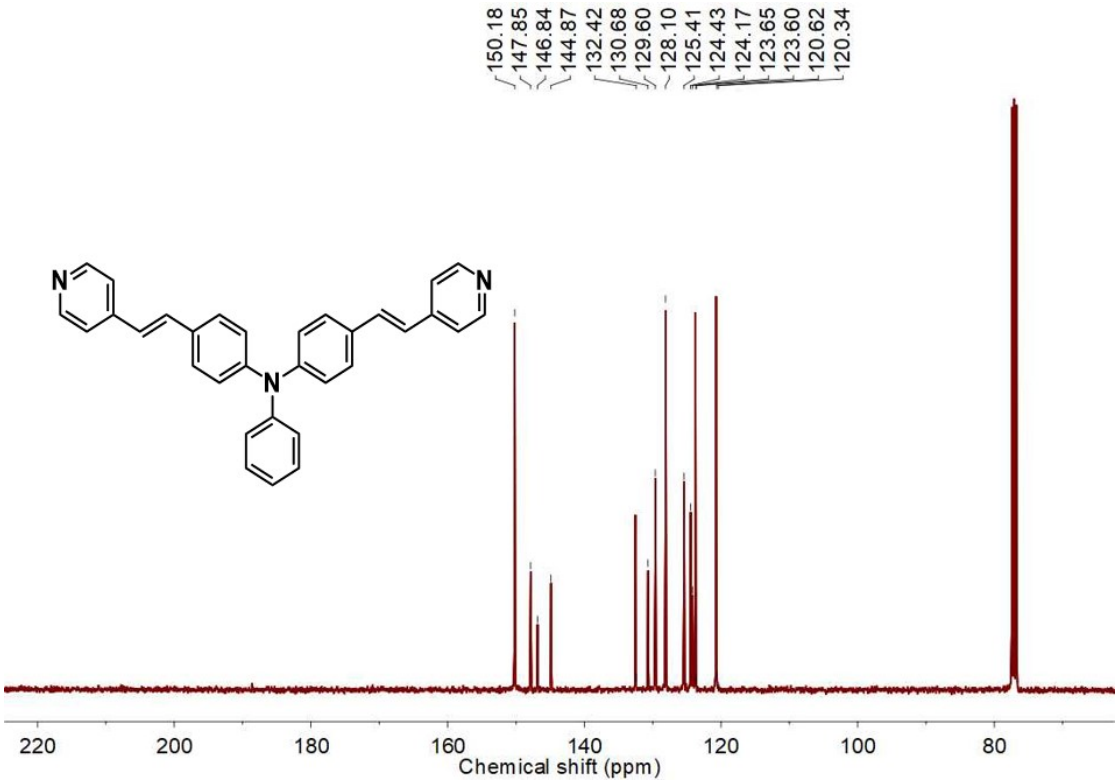

Figure S4. ^{13}C NMR spectrum of **TPA-DPy** in $CDCl_3$

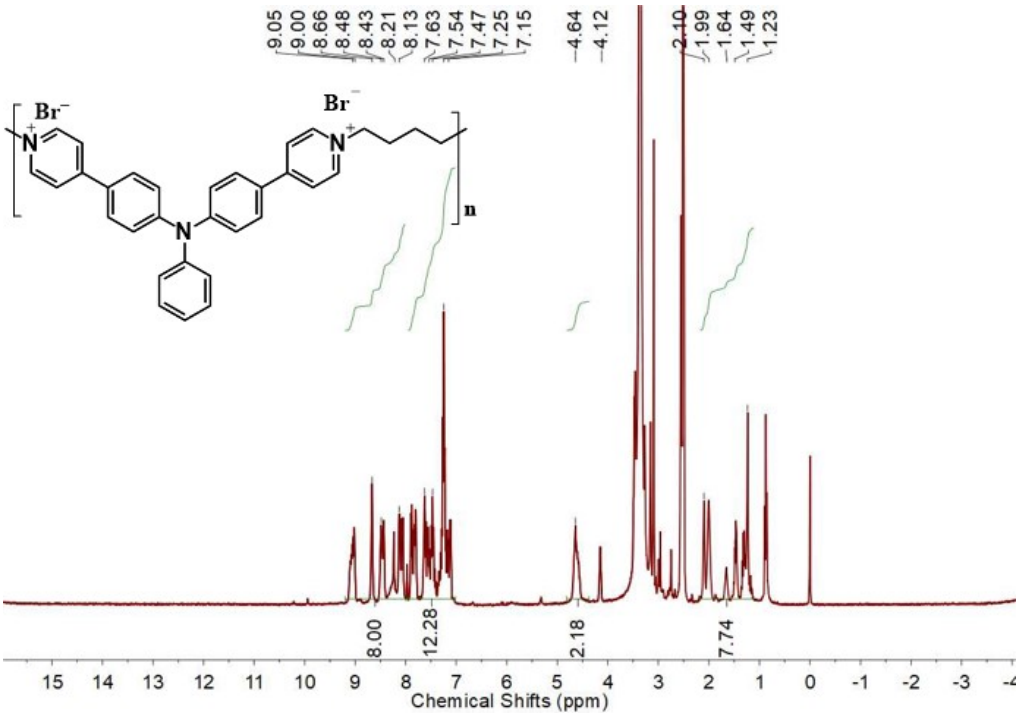

Figure S5. ^{1}H NMR spectrum of **TPA-SPy-4** in DMSO-d_6

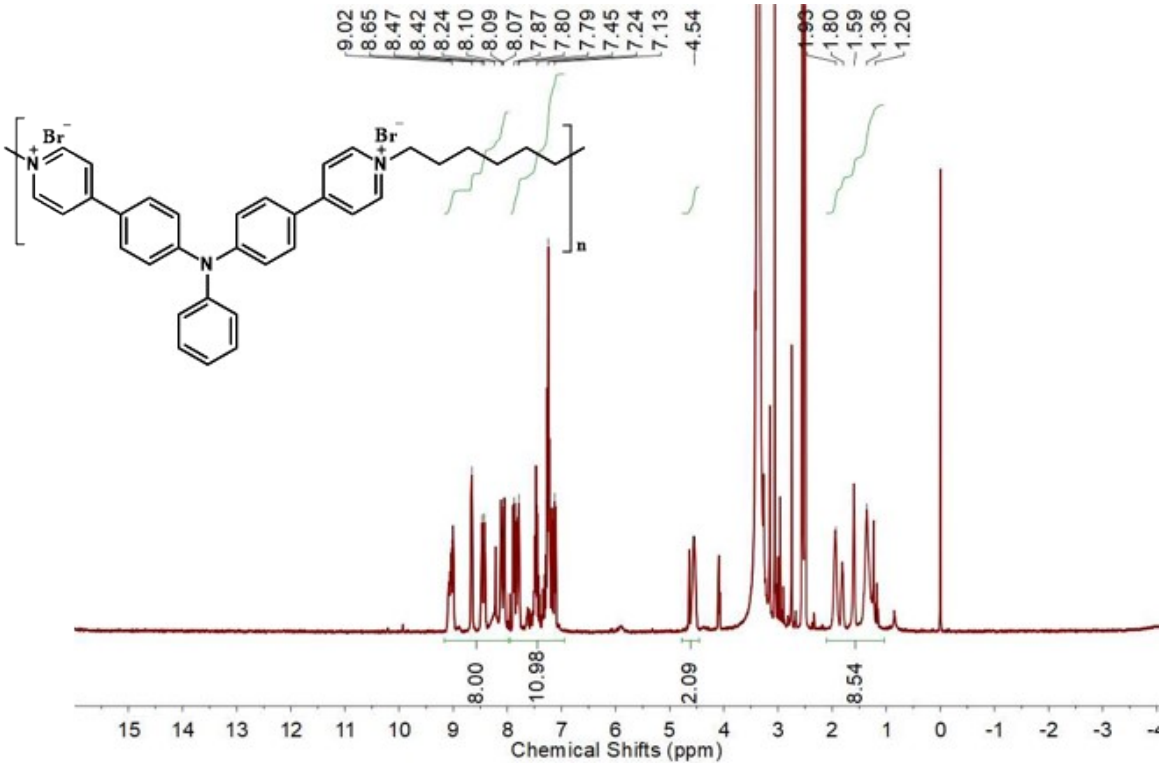

Figure S6. ^{1}H NMR spectrum of **TPA-SPy-6** in DMSO-d_6

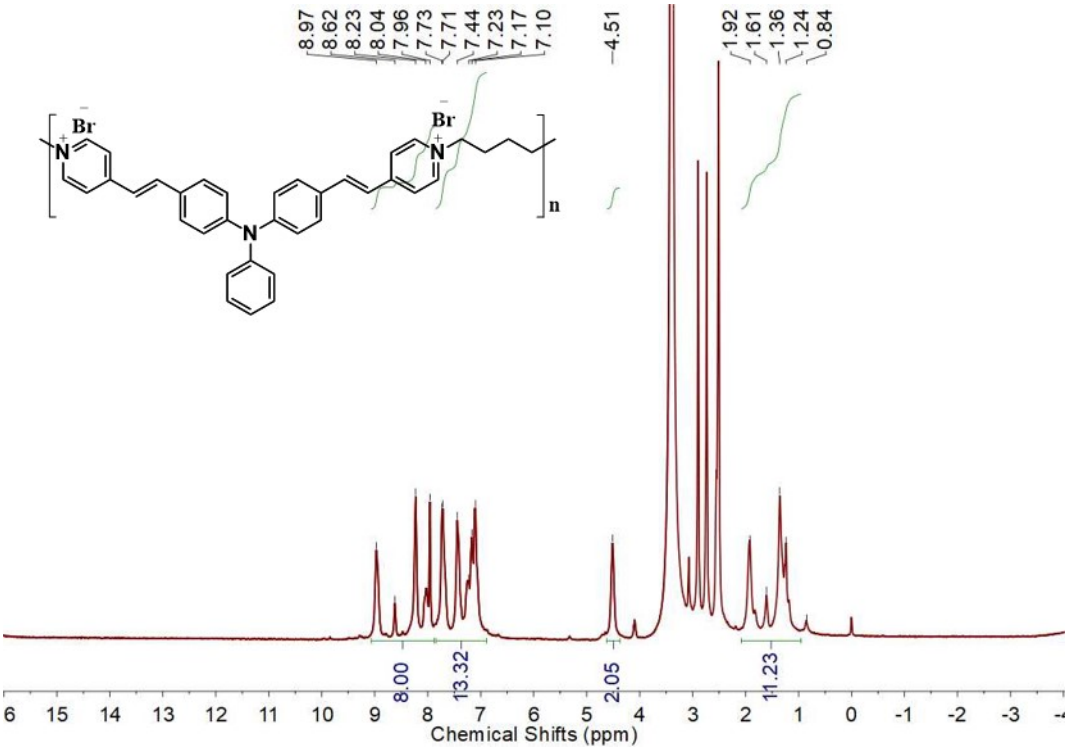

Figure S7. ^{1}H NMR spectrum of **TPA-DPy-4** in DMSO-d_6

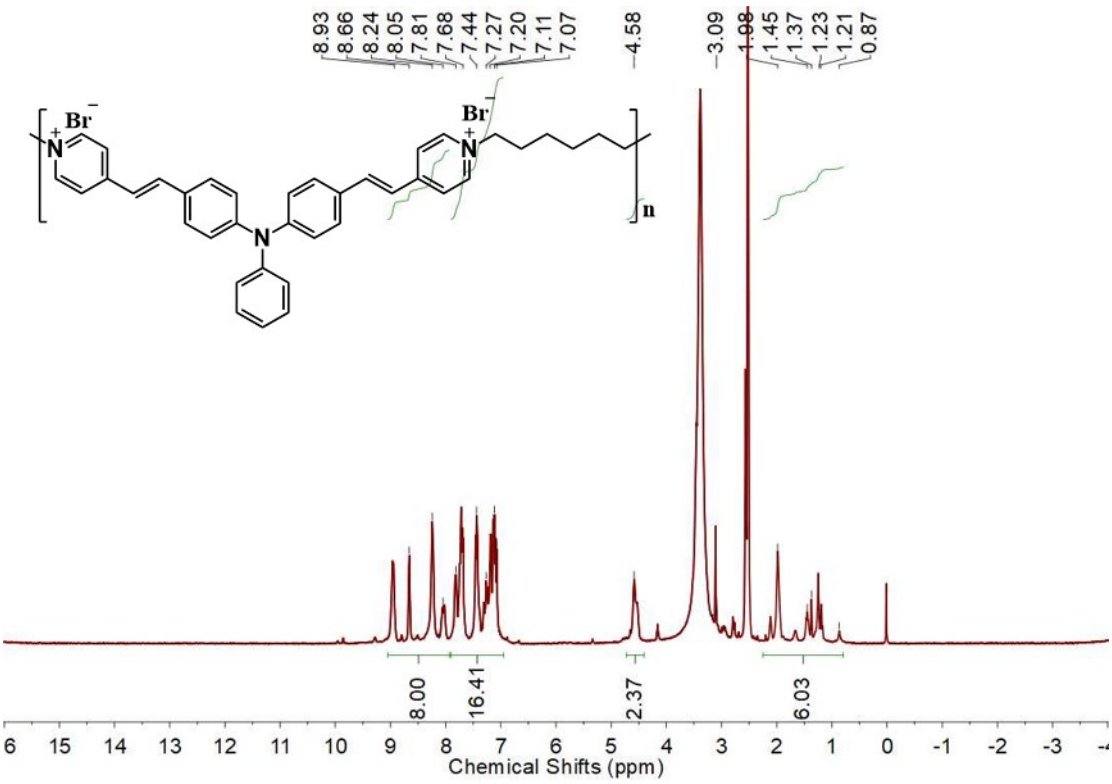

Figure S8. ^{1}H NMR spectrum of **TPA-DPy-6** in DMSO-d_6

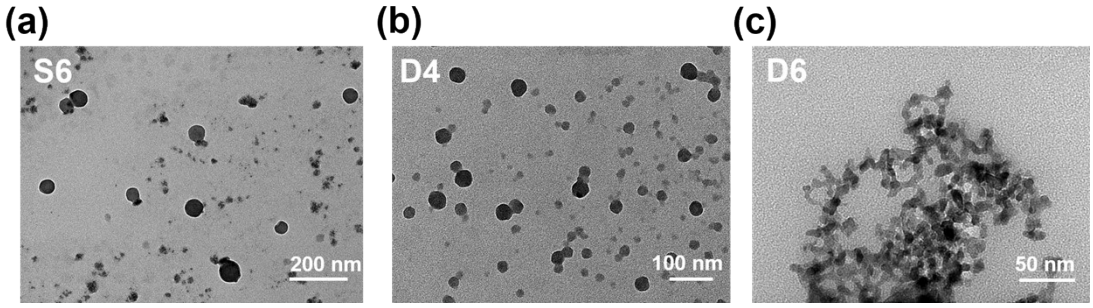

Figure S9. TEM images of **TPA-SPy-6**, **TPA-DPy-4** and **TPA-DPy-6,** scale bar: 200, 100, 50 nm, respectively.

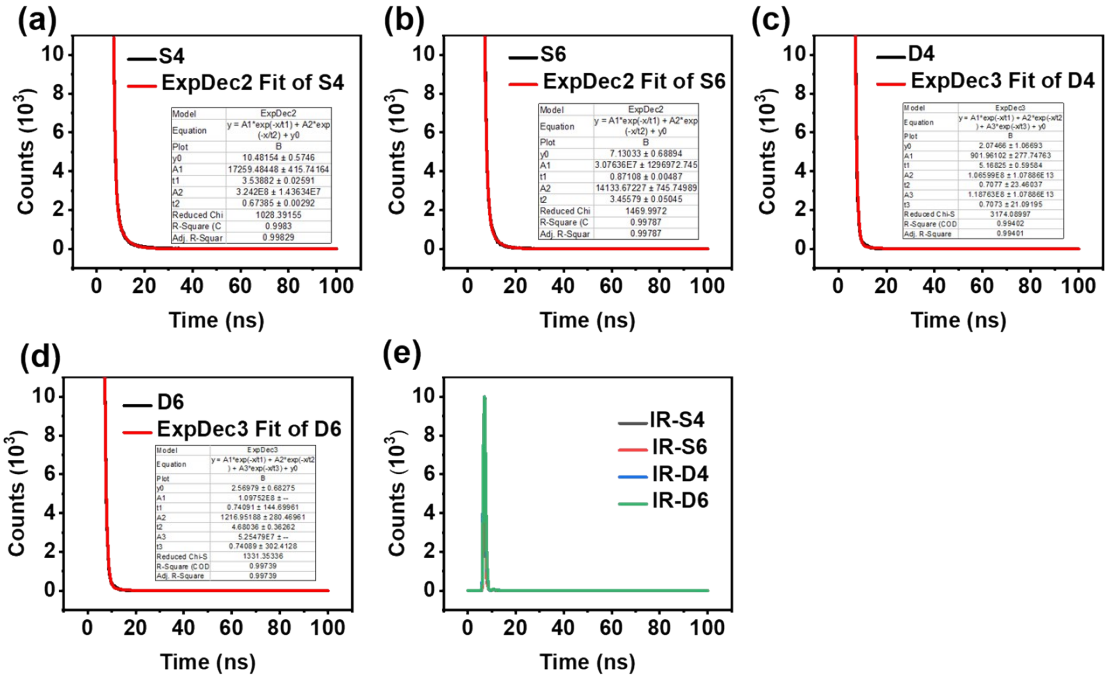

Figure S10. Transient fluorescence spectra and fitting curve curves of the samples and IRF data of the tests.

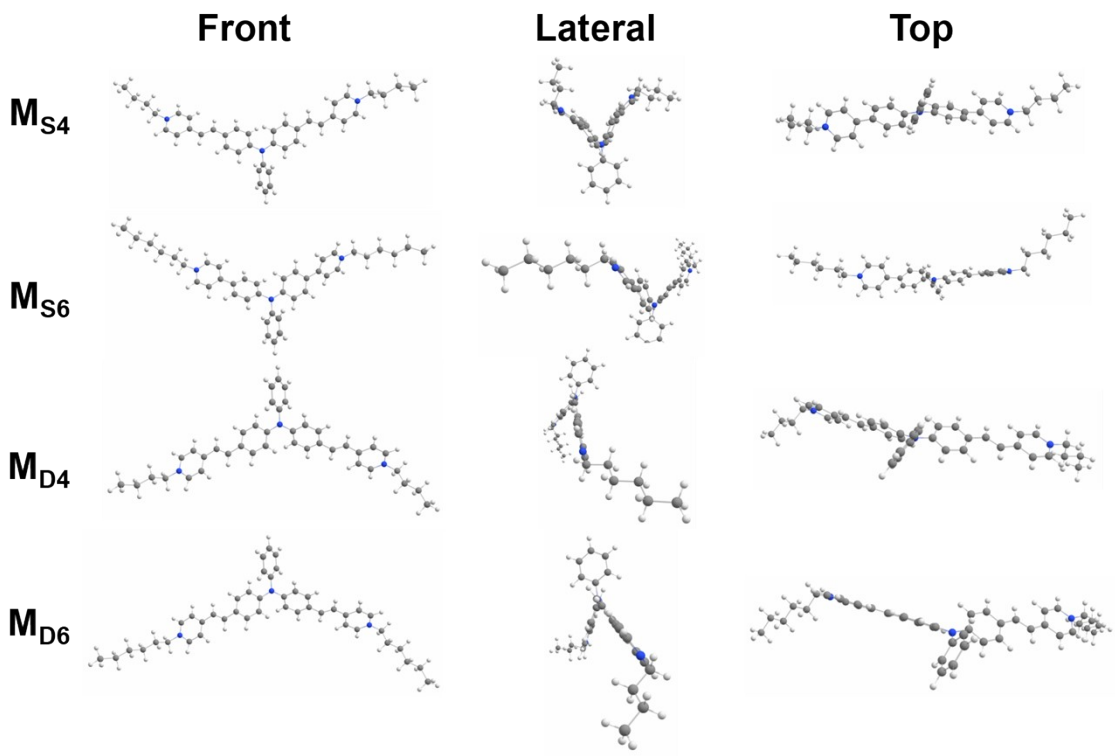

Figure S11. Optimized configuration of the model molecules.

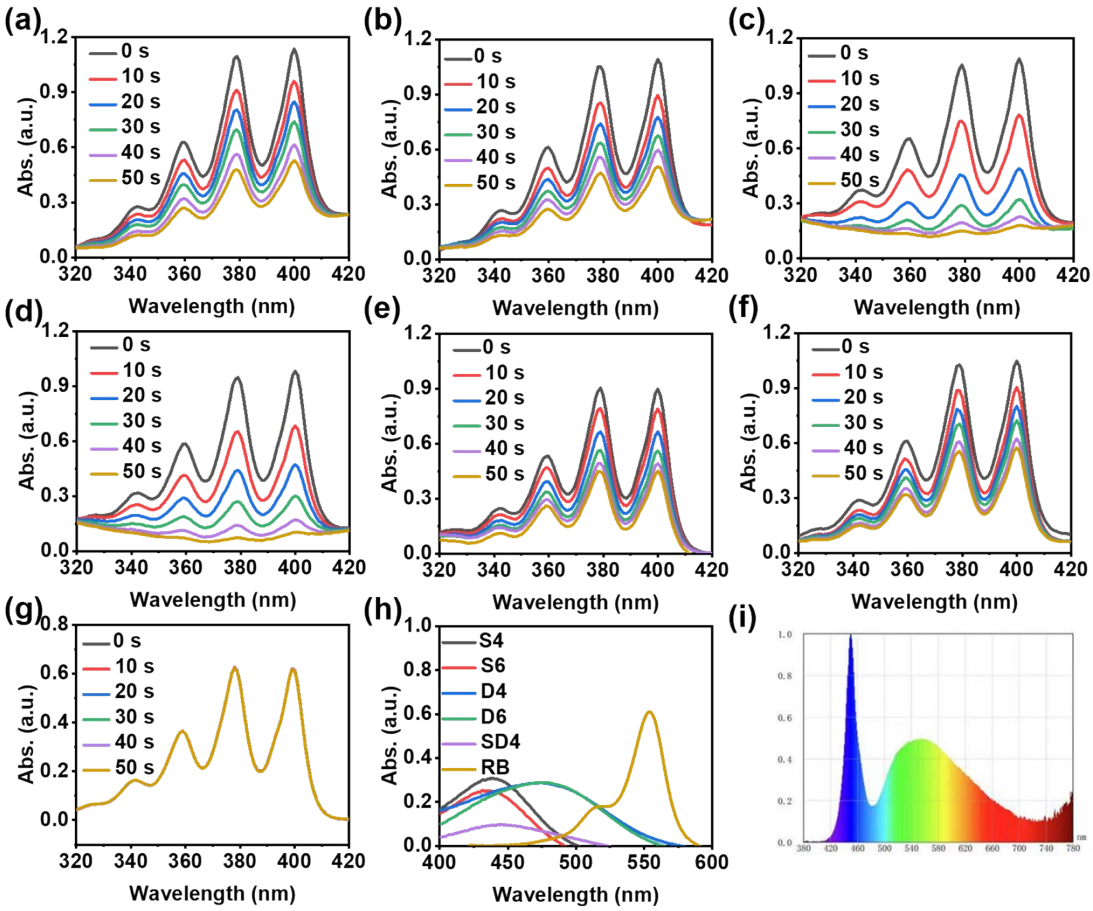

Figure S12. ABDA decomposition curves under white light irradiation (70 mW cm-

2) for different groups, including (**a**) **S4**, (**b**) **S6**, (**c**) **D4**, (**d**) **D6,** (**e**) **SD4**, **(f)** Rose Bengal and (**g**) control (C_{sample} = 10 μM, C_{ABDA} = 100 μM.); (**h**) the actual UV/vis absorption spectra of the samples; (**i**) the spectrum of the LED while light provided by the seller.

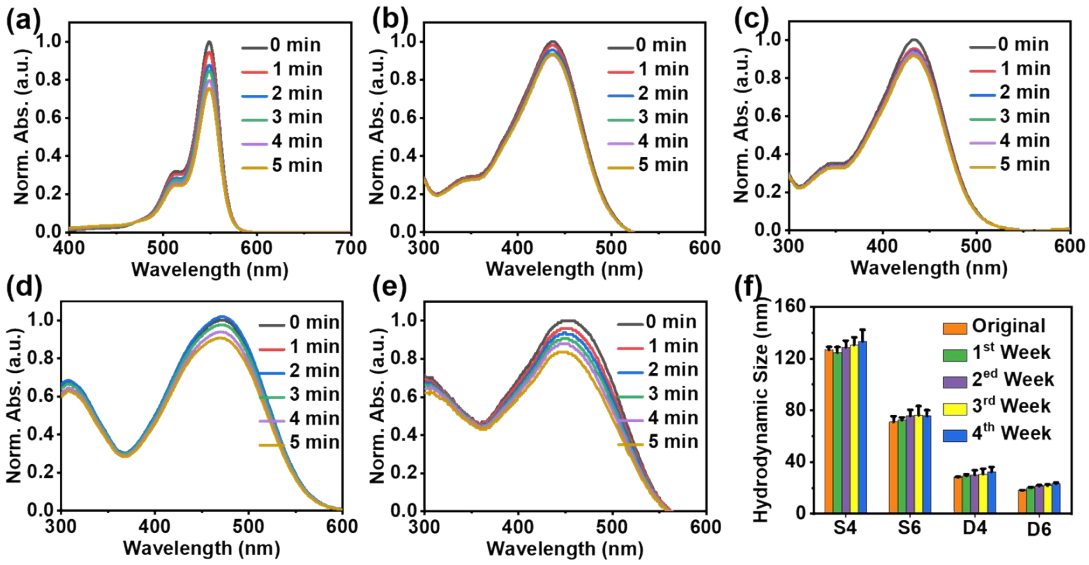

Figure S13. UV/vis absorption spectra of the sample under white light illumination (70 mW/cm^2). (**a**) Rose Bengal, (**b**) S4, (**c**) S6, (**d**) D4, (**e**) D6; (**f**) hydrodynamic diameter changes of the samples when stored in refrigerator (4 °C).

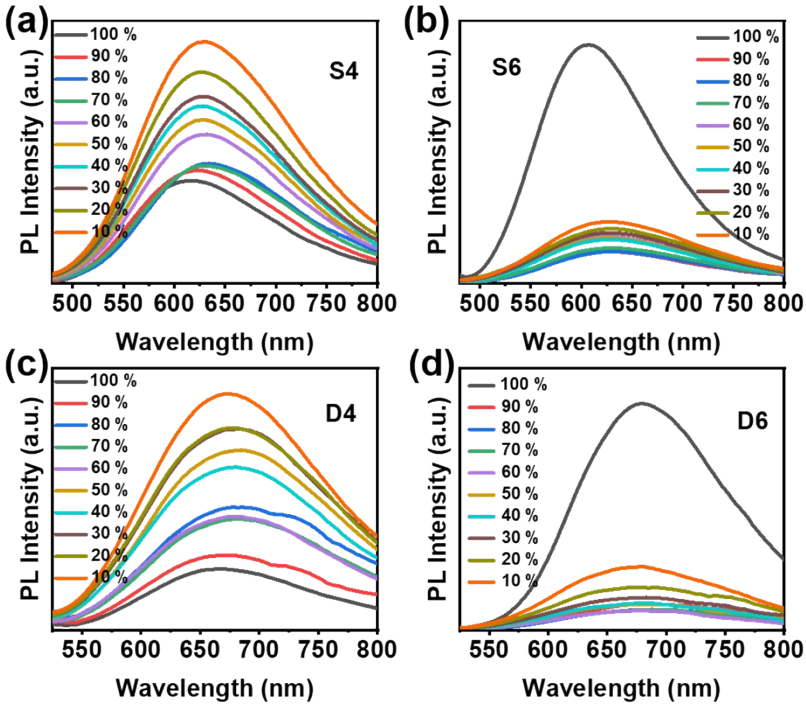

Figure S14. PL spectra of (**a**) **S4**, (**b**) **S6**, (**c**) **D4** and (**d**) **D6** in THF/water mixture with varying amount of THF.

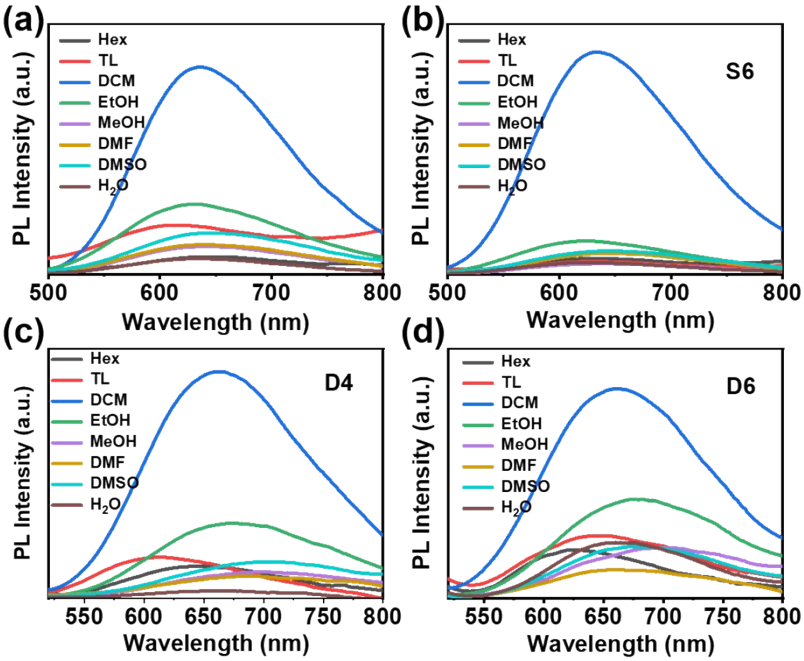

Figure S15. PL spectra of (**a**) **S4**, (**b**) **S6**, (**c**) **D4** and (**d**) **D6** in solvent with different polarity.

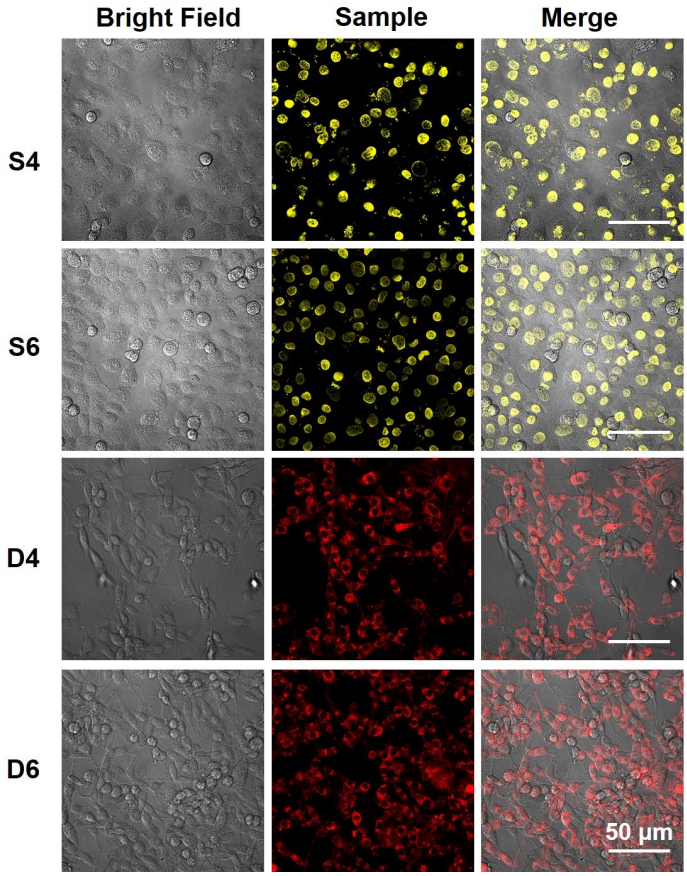

Figure S16. CLSM images of A549 cancer cells incubated with **S4** and **S6** for 12 h, and U87 cancer cell incubated with **D4** and **D6** for 12 h.

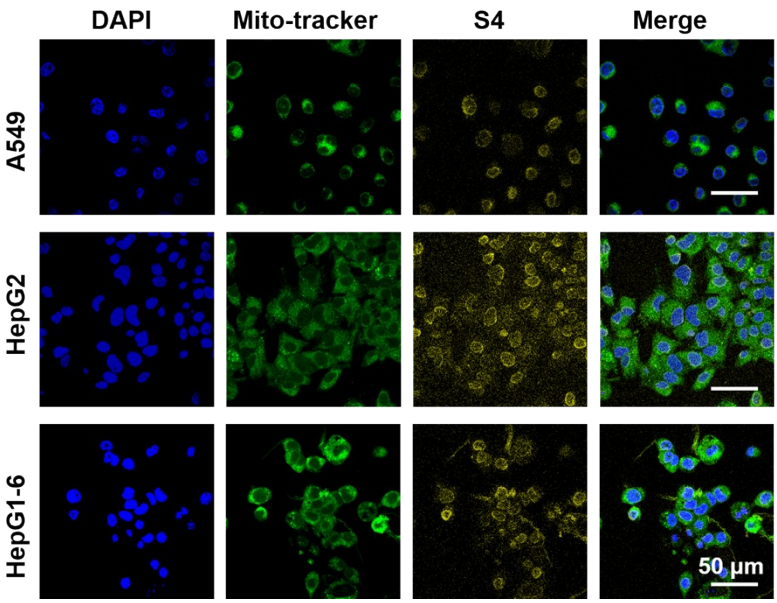

Figure S17. CLSM images of A540 cancer cell, HepG2 cancer cells, and HepG1-6 cancer cell incubated with **S4** for 12 h, from which we can see that **S4** preferentially accumulates at nucleus for all cells (C_{S4}: 2 μM, scale bar: 50 μm).

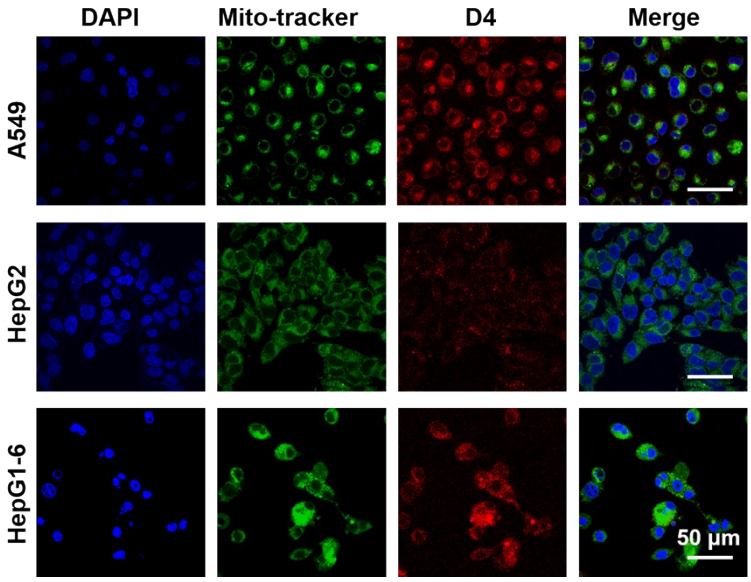

Figure S18. CLSM images of A540 cancer cell, HepG2 cancer cells, and HepG1-6 cancer cell incubated with **D4** for 12 h, from which we can see that **D4** preferentially accumulates at cytoplasm and overlaps with mito-tracker for all cells (C_{D4}: 2 μM, scale bar:50 μm).

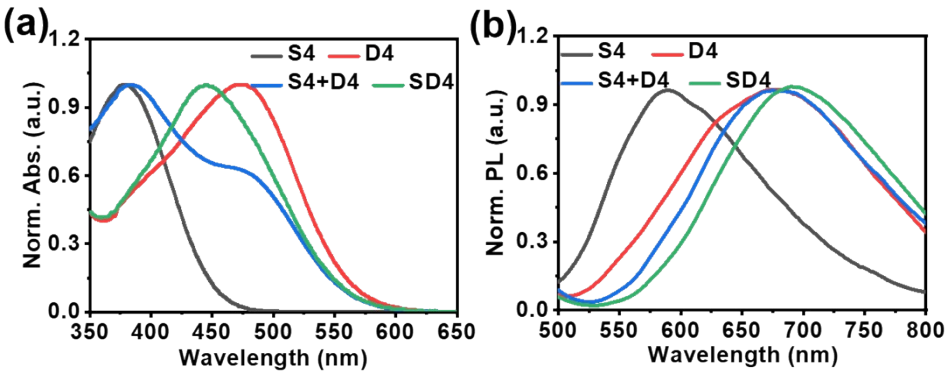

Figure S19. UV/vis of the sample obtained during the preparation of **SD4**. The absorption spectra seem to be merely the addition of **S4** and **D4**, while the spectroscopy of **SD4** becomes a new one, implying the its homogenization. The bule shift of the spectra of **S4** and **D4** in comparison with initial testing might arise from the changed DMSO/water ratio.

Table S2 Summary of therapeutic efficacy of some organelle-targeting PDT agent.

Sample name	Organelle	Cell line	Cell viability at 2 μM	reference
TBD-3C	Plasma Membrane	Hela	~ 100%	2
TPETSAI	Plasma Membrane	MDA-MB-231	~ 80%	3
Chimeric peptide nanorods	Plasma Membrane and nucleus	4T1, Hela	~40%-50%	4
Chimeric peptide	Plasma Membrane, Mitochondria	4T1, COS7	>60%	5
P-PplX	Plasma Membrane	4T1	~90%	6
TTVP	Plasma Membrane	Hela	~10%	7
TPANPF6	Mitochondria	Hela	>80%	8
TPA-DT-Qy	Mitochondria	MCF-7, MDA-MB-231	~20%	9
AIE-Br	Mitochondria	Hela	~30%	10
TPATrzPy-3+	Mitochondria	Hela	~80%	11
HIM-MnO2	Mitochondria	4T1, B16F10	~60%	12
TPECM2TPP	Mitochondria	Hela	~40%	13
ICG+HAuNS	Endoplasmic Reticulum	CT-26	~90%	14
Ir-Es, Ir-Me	Nucleus	HepG2	~90%	15
TFPy, TFVP, TPE-TFPy three in one	Mitochondria, Plasma Membrane, Lysosome	Hela	>60%	16
TPA-TPP-MeO	Mitochondria, Lysosome	Hela	~80%-90%	17
TPA-2PI	Mitochondria	4T1	~5%	18
S4+D4	Nucleus, Mitochondria	U87	14%	This work

Reference

1. S. S. Zhao, L. Wang, Y. Liu, L. Chen and Z. Xie, Stereochemically Dependent Synthesis of Two Cu(I) Cluster-Based Coordination Polymers with Thermochromic Luminescence, *Inorg. Chem.*, 2017, **56**, 13975-13981.
2. M. Wu, X. Liu, H. Chen, Y. Duan, J. Liu, Y. Pan and B. Liu, Activation of Pyroptosis by Membrane-Anchoring AIE Photosensitizer Design: New Prospect for Photodynamic Cancer Cell Ablation, *Angew. Chem. Int. Ed. Engl.*, 2021, **60**, 9093-9098.
3. Y. Yuan, S. Xu, X. Cheng, X. Cai and B. Liu, Bioorthogonal Turn-On Probe Based on Aggregation-Induced Emission Characteristics for Cancer Cell Imaging and Ablation, *Angew. Chem. Int. Ed. Engl.*, 2016, **55**, 6457-6461.
4. H. Cheng, P. Yuan, G. Fan, L. Zhao, R. Zheng, B. Yang, X. Qiu, X. Yu, S. Li and X. Zhang, Chimeric peptide nanorods for plasma membrane and nuclear targeted photosensitizer delivery and enhanced photodynamic therapy, *Appl. Mater. Today*, 2019, **16**, 120-131.
5. H. Cheng, R. R. Zheng, G. L. Fan, J. H. Fan, L. P. Zhao, X. Y. Jiang, B. Yang, X. Y. Yu, S. Y. Li and X. Z. Zhang, Mitochondria and plasma membrane dual-targeted chimeric peptide for single-agent synergistic photodynamic therapy, *Biomaterials*, 2019, **188**, 1-11.
6. G. L. Fan, F. A. Deng, X. Zhou, L. S. Liu, J. Q. Huang, D. W. Zhang, Y. X. Sun, A. L. Chen, H. Cheng and S. Y. Li, Plasma membrane targeted photodynamic O2 economizer for hypoxic tumor therapy, *Biomaterials*, 2021, **273**, 120854.
7. D. Wang, H. Su, R. T. K. Kwok, X. Hu, H. Zou, Q. Luo, M. M. S. Lee, W. Xu, J. W. Y. Lam and B. Z. Tang, Rational design of a water-soluble NIR AIEgen, and its application in ultrafast wash-free cellular imaging and photodynamic cancer cell ablation, *Chem. Sci.*, 2018, **9**, 3685-3693.
8. Z. Liu, H. Zou, Z. Zhao, P. Zhang, G. G. Shan, R. T. K. Kwok, J. W. Y. Lam, L. Zheng and B. Z. Tang, Tuning Organelle Specificity and Photodynamic Therapy Efficiency by Molecular Function Design, *ACS Nano*, 2019, **13**, 11283-11293.
9. G. Yuan, C. Lv, J. Liang, X. Zhong, Y. Li, J. He, A. Zhao, L. Li, Y. Shao, X. Zhang, S. Wang, Y. Cheng and H. He, Molecular Engineering of Efficient Singlet Oxygen Generators with Near‐Infrared AIE Features for Mitochondrial Targeted Photodynamic Therapy, *Adv. Funct. Mater.*, 2021, **31**.
10. Q. Hu, M. Gao, G. Feng and B. Liu, Mitochondria-targeted cancer therapy using a light-up probe with aggregation-induced-emission characteristics, *Angew. Chem. Int. Ed. Engl.*, 2014, **53**, 14225-14229.
11. Y. Wang, S. Xu, L. Shi, C. Teh, G. Qi and B. Liu, Cancer-Cell-Activated in situ Synthesis of Mitochondria-Targeting AIE Photosensitizer for Precise

Photodynamic Therapy, *Angew. Chem. Int. Ed. Engl.*, 2021, **60**, 14945-14953.
12. H. Ren, Q. Yang, J. Yong, X. Fang, Z. Yang, Z. Liu, X. Jiang, W. Miao and X. Li, Mitochondria targeted nanoparticles to generate oxygen and responsive-release of carbon monoxide for enhanced photogas therapy of cancer, *Biomater. Sci.*, 2021, **9**, 2709-2720.
13. C. J. Zhang, Q. Hu, G. Feng, R. Zhang, Y. Yuan, X. Lu and B. Liu, Image-guided combination chemotherapy and photodynamic therapy using a mitochondria-targeted molecular probe with aggregation-induced emission characteristics, *Chem. Sci.*, 2015, **6**, 4580-4586.
14. W. Li, J. Yang, L. Luo, M. Jiang, B. Qin, H. Yin, C. Zhu, X. Yuan, J. Zhang, Z. Luo, Y. Du, Q. Li, Y. Lou, Y. Qiu and J. You, Targeting photodynamic and photothermal therapy to the endoplasmic reticulum enhances immunogenic cancer cell death, *Nat. Commun.*, 2019, **10**, 3349.
15. X. Tian, Y. Zhu, M. Zhang, L. Luo, J. Wu, H. Zhou, L. Guan, G. Battaglia and Y. Tian, Localization matters: a nuclear targeting two-photon absorption iridium complex in photodynamic therapy, *Chem. Commun. (Camb)*, 2017, **53**, 3303-3306.
16. W. Xu, M. M. S. Lee, J. J. Nie, Z. Zhang, R. T. K. Kwok, J. W. Y. Lam, F. J. Xu, D. Wang and B. Z. Tang, Three-Pronged Attack by Homologous Far-red/NIR AIEgens to Achieve 1+1+1>3 Synergistic Enhanced Photodynamic Therapy, *Angew. Chem. Int. Ed. Engl.*, 2020, **59**, 9610-9616.
17. Y. Ma, Z. Zhuang, L. Xing, J. Li, Z. Yang, S. Ji, R. Hu, Z. Zhao, Y. Huo and B. Z. Tang, The AIE-Active Dual-Cationic Molecular Engineering: Synergistic Effect of Dark Toxicity and Phototoxicity for Anticancer Therapy, *Adv. Funct. Mater.*, 2021, **31**.
18. Y. Zhou, W. Xia, C. Liu, S. Ye, L. Wang and R. Liu, A DNA and mitochondria dual-targeted photosensitizer for two-photon-excited bioimaging and photodynamic therapy, *Biomater. Sci*, 2022, **10**, 1742-1751.